

Supporting Information

Linking the Enhanced Deep NO Oxidation of Ferroelectric $\text{K}_{0.5}\text{Bi}_{0.5}\text{TiO}_3$ Nanowire Photocatalyst to Its Spontaneous Polarization and Oxygen Vacancies

Qingrong Liang^a, Guian Li^{a,*}, Fei Rao^a, Guozhong Zheng^a, Haoxuan Ma^a, Shiping Li^a, Jian Zhang^a, Mirabbos Hojamberdiev^b, Qizhao Wang^c and Gangqiang Zhu^{a,*}

^a*School of Physics and Information Technology, Shaanxi Normal University, Xi'an 710061, PR China*

^b*Institut für Chemie, Technische Universität Berlin, Straße des 17. Juni 135, 10623 Berlin, Germany*

^c*School of Environmental Science and Engineering, Chang'an University, Xi'an 710064, P.R. China*

*Corresponding author:

E-mail addresses: liguian@snnu.edu.cn (G. Li), zgq2006@snnu.edu.cn (G. Zhu)

1.1. Photocatalytic NO removal test

The photocatalytic NO removal tests were conducted at room temperature in a continuous flow reactor. The volume of the stainless steel reactor covered with a quartz glass was 4.5 L (10 × 30 × 15 cm). The glass substrate with a photocatalytic film was placed in the center of the reactor. A 300 W Xenon lamp with a 420-nm cutoff filter was used as a visible light source. The visible light source was vertically placed 20 cm above the glass substrate. The photocatalytic film was prepared by dispersing 0.1 g of $K_{0.5}Bi_{0.5}TiO_3$ nanowires in 15 mL of deionized water under ultrasonication for 15 min, depositing the photocatalytic paste onto the glass substrate ($d = 10$ cm) by drop casting and drying at 70°C for 4 h.

The concentration of NO+air mixture gas was 430 ppb. The mixture gas was produced by diluting NO feed stream (50 ppm) with zero air in the gas dilution calibrator (Model 4010, Sabio). The entire measurement was conducted at ambient conditions with relative humidity of 30±5%. When the adsorption-desorption equilibrium was achieved, the photocatalytic film was irradiated by visible light. The concentration of NO was continuously detected and measured every one minute using a NO-NO₂-NO_x analyzer (Model 42i, ThermoFischer Scientific). The removal rate (η) of NO was calculated using the following equation:

$$\eta = 1 - \left(\frac{c}{c_0} \right) \times 100\% \quad (1)$$

where C and C_0 refer to the NO concentrations at a given time and initial concentration, respectively.

1.2. In situ FTIR spectroscopy

The FTIR spectra were recorded on a VERTEX 70 spectrometer (Bruker) equipped with an *in situ* reaction chamber, gas system, light source, and pretreatment equipment. Before starting the adsorption process, the photocatalyst sample was purged by high-purity He for 1 h at 150°C to clean the photocatalyst surface, and then the baseline was collected after cooling to 30°C. Afterward, the

gas mixture ($15 \text{ mL} \cdot \text{min}^{-1}$ NO (50 ppm) and $30 \text{ mL} \cdot \text{min}^{-1}$ O₂) was inserted into the reaction chamber. In the dark, NO was adsorbed on the photocatalyst surface for 20 min, and then the photocatalyst was irradiated by visible light for 30 min. The FTIR spectra in the wavenumber range of $4000\text{-}600 \text{ cm}^{-1}$ were recorded every two minutes in the dark and every three minutes under visible light irradiation.

1.3. Theoretical calculations

Density functional theory (DFT) calculations were implemented using the Cambridge Sequential Total Energy Package (CASTEP) code [1]. The super cell models of K_{0.5}Bi_{0.5}TiO₃ with oxygen vacancies (OVs) were built, and the super cells of $1 \times 1 \times 1$ were used for all samples. The crystal models of K_{0.5}Bi_{0.5}TiO₃ with interfaces of the (001) crystallographic planes were also constructed. The generalized gradient approximation with the Perdew-Burke-Ernzerhof exchange-correlation density functional was used to account for exchange correlation potentials and electron-electron interactions [2]. The Brillouin zones were separately sampled at $1 \times 3 \times 1$ Monkhorst-Pack *k*-points for the crystal models. The kinetic cutoff energy was set to 380 eV for all calculations, and the self-consistent field convergence criterion was set to 2.0×10^{-6} eV. For geometry optimization, energy change, residual force, stress and displacement convergence criteria were chosen to be less than 2.0×10^{-5} eV atom⁻¹, 0.05 eV Å⁻¹, 0.1 GPa, and 0.002 Å, respectively. The charge transfer was evaluated based on electron density difference (EDD) maps and Mulliken population analysis (MPA) performed using a $2 \times 4 \times 2$ mesh.

Table S1. Assignments of FTIR bands observed during photocatalytic NO oxidation process over KBT-O under visible light irradiation.

Wavenumber, cm^{-1}	Assignment
1022, 1249, 1309, 1448 and 1540	$bi\text{-NO}_3^-$
1056, 1207 and 1623	$br\text{-NO}_3^-$
1064, 1259 and 1347	$m\text{-NO}_3^-$
1097, 1182, 1249, 1425 and 1309	NO_2^-
1727 and 1461	NO_2
1376 and 1373	N_2O_4
1698	NO^+

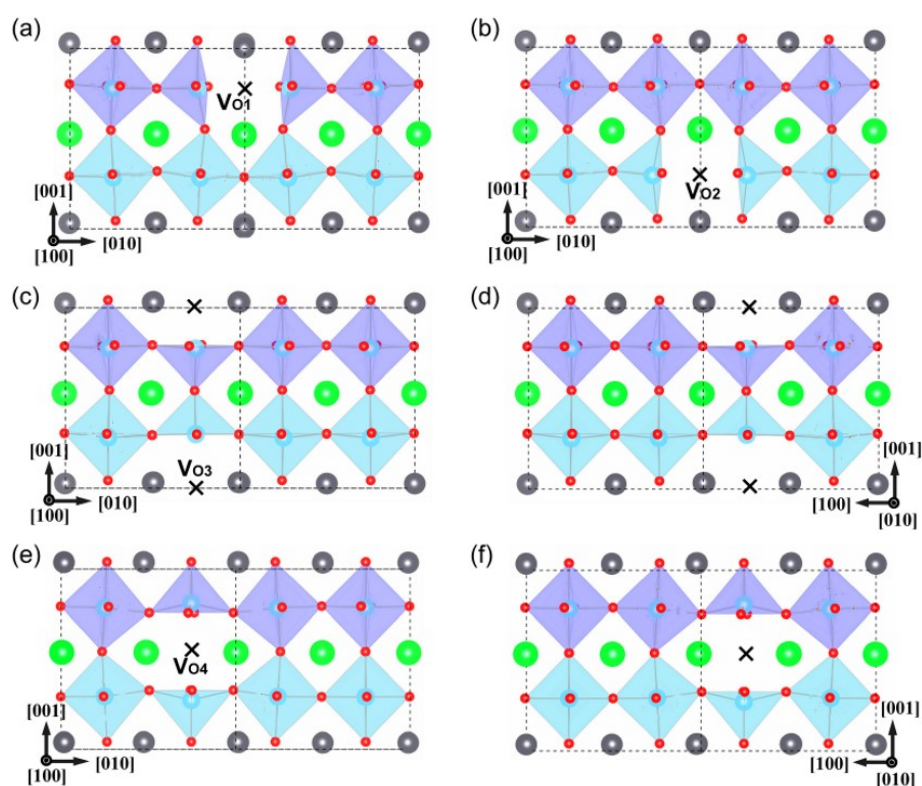


Figure S1. Schematic representation of the positions of oxygen vacancies in the BO₆ of KBT. (a,b) Projection of O1 and O2 vacancies on the (100) crystallographic plane and rotation of oxygen octahedron around the [100] axis. (c,d) Projection of O3 vacancy on the (100) crystallographic plane, schematic diagram of the (010) crystallographic plane and rotation of different oxygen octahedra along the [100] axis or [010] axis. (e,f) Projection of O4 vacancy on the (100) and (010) crystallographic planes, and rotation of different oxygen octahedra along the [100] axis or the [010] axis.

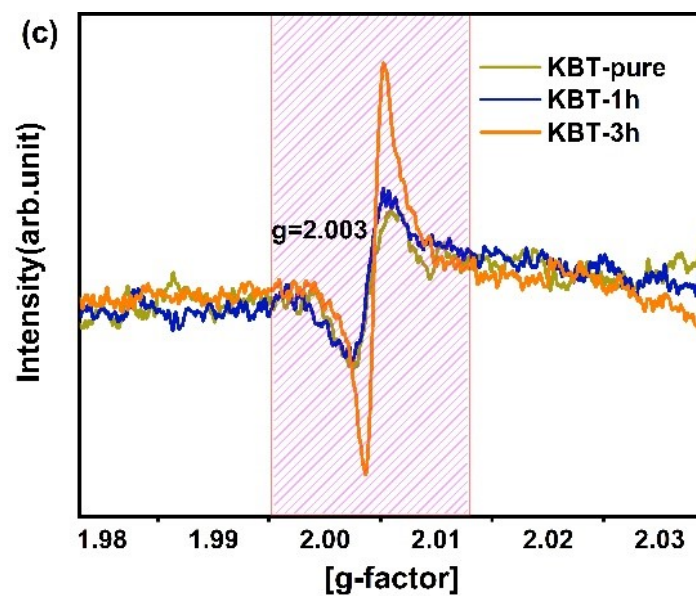


Figure S2. EPR spectra of KBT-P, KBT-O-1H, and KBT-O-3H.

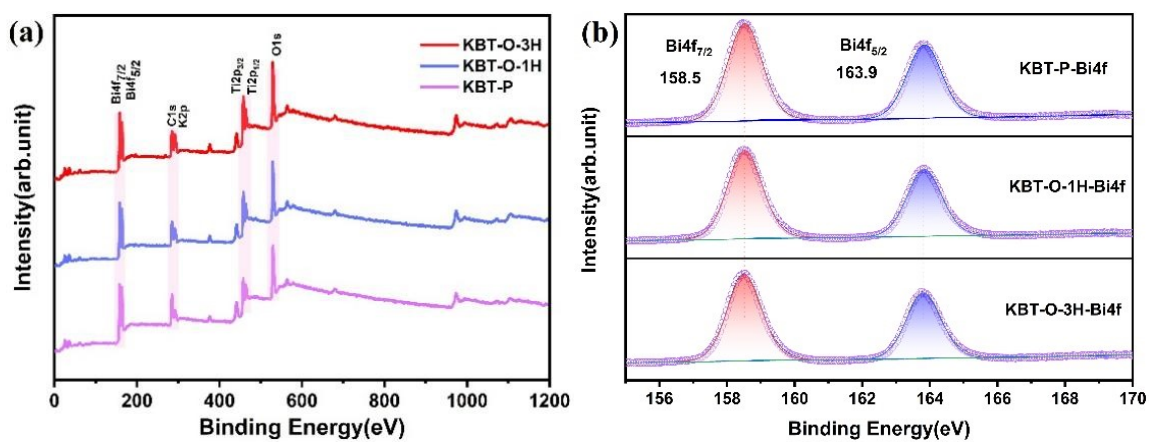


Figure S3. (a) XPS survey spectra and (b) Bi 4f XPS spectra of KBT-P, KBT-O-1H, and KBT-O-3H.

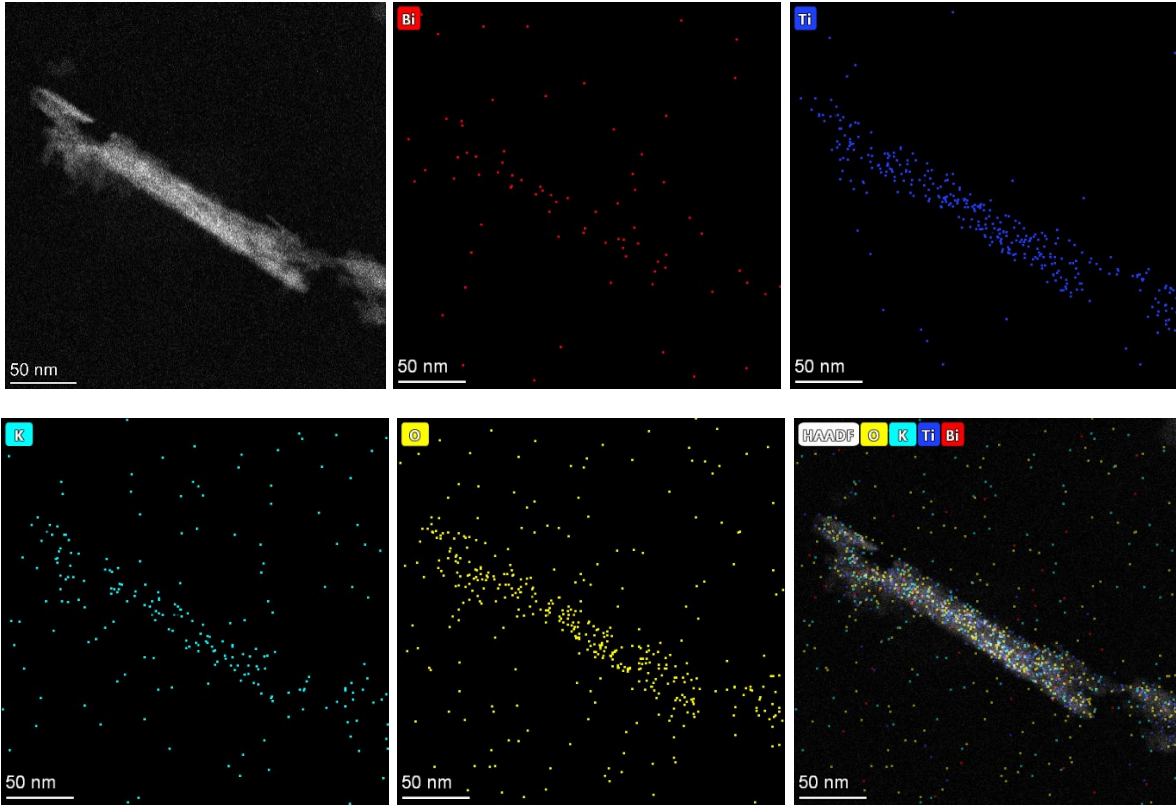


Figure S4. EDX element mapping images of KBT-O-3H.

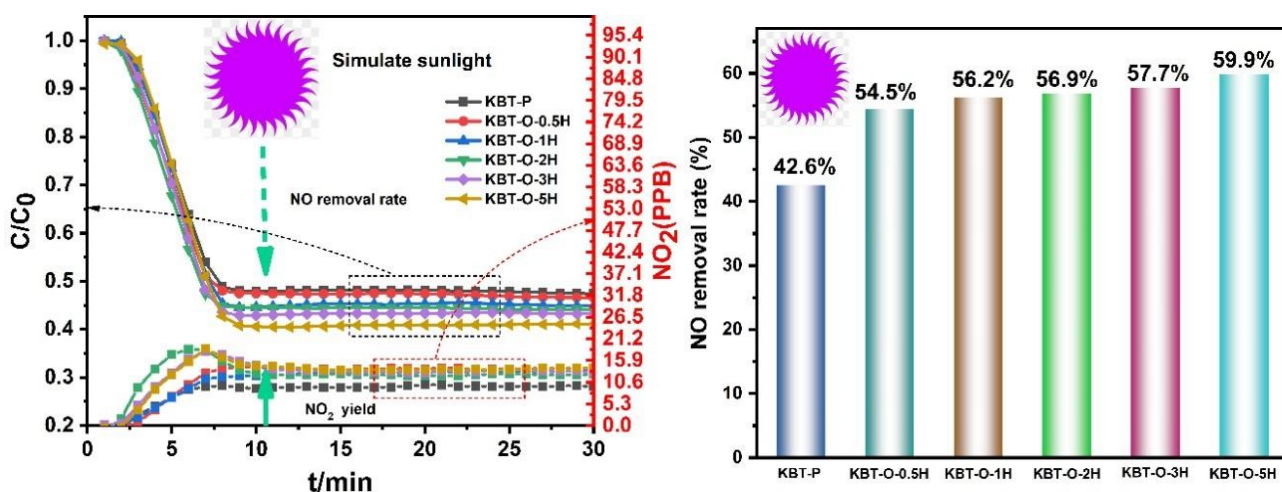


Figure S5. (a) Photo-oxidative removal of NO and NO_2 generation and (b) NO removal rate of KBT-P, KBT-O-0.5H, KBT-O-1H, KBT-O-2H, KBT-O-3H, and KBT-O-5H under simulated sunlight.

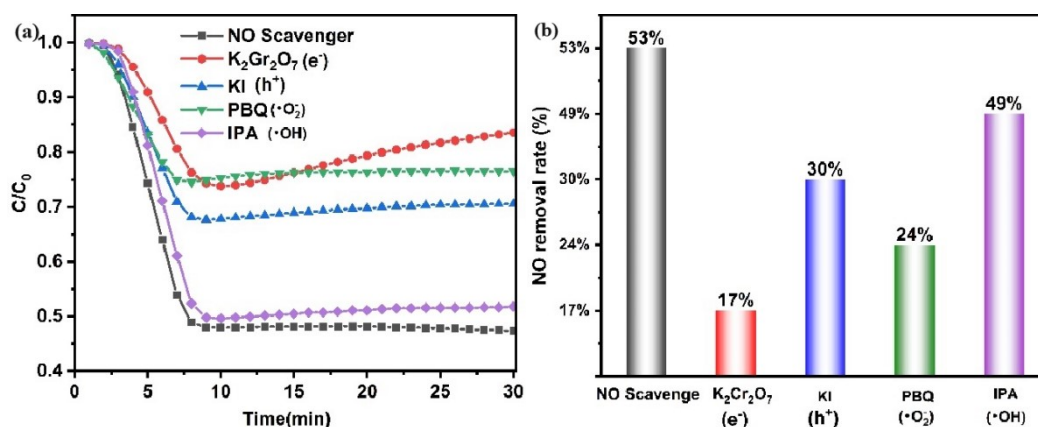


Figure S6 (KBT-O-3H capture experiment; (b) the NO removal efficiency of each capture agent.

In order to reveal the depletion and effect of photogenerated carries and reactive species, including photoinduced e^- , h^+ , hydroxyl radicals and superoxide species, the trapping experiments with $K_2Cr_2O_7$, KI, PBQ, and IPA as scavengers are conducted over the KBT-O-3H sample. Obviously, the addition of $K_2Cr_2O_7$ and PBQ significantly decreased the photocatalytic activity of NO removal, the addition of KI played an inhibitory effect as well. While the photocatalytic performance only minor decrease after the $\cdot OH$ species were captured by IPA. As shown in Figure S6b, the photocatalytic efficiency of KBT-O-3H with addition of $K_2Cr_2O_7$, KI, PBQ, and IPA are 17, 30, 24, and 49% for NO removal, respectively. These trapping agents inhibit the catalytic activity of the catalyst to varying degrees. The photogenerated electrons play the most important effect on NO removal. As the trapping of the photo-generated holes and $\cdot O_2^-$ radicals by corresponding agents the removal rate of NO over

KBT-O-3H decrease to 30% and 24%. It means that photo-generated holes and $\bullet\text{O}_2^-$ radicals also restrict the NO photo-oxidation process over the KBT-O-3H sample. The similar removal rate between KBT-O-3H without scavenge agents and KBT-O-3H with IPA scavenge agents implies that $\bullet\text{OH}$ species have a minimal effect on the photocatalytic reactions.

REFERENCES

- (1) Perdew, J.P.; Burke, K.; Ernzerhof, M. Generalized Gradient Approximation Made Simple. *Phys. Rev. Lett.* **1996**, 77, 3865–3868.
- (2) Segall, M. D.; Lindan, P. J. D.; Probert, M. J.; Pickard, C. J.; Hasnip, P. J.; Clark, S. J.; Payne, M. C. First-principles Simulation: Ideas, Illustrations and The CASTEP Code. *J.Phys.:Condens. Matter* **2002**, 14, 2717–2744.
- (3) Tonda, S.; Kumar, S.; Bhardwaj, M.; Yadav, P.; Ogale, S. g-C₃N₄/NiAl-LDH 2D/2D Hybrid Heterojunction for High-Performance Photocatalytic Reduction of CO₂ into Renewable Fuels. *ACS Appl. Mater. Interfaces* **2018**, 10, 2667–2678.